Recent Earth Oblateness Variations: Unraveling Climate and Postglacial Rebound Effects

Jean O. Dickey,[1]* Steven L. Marcus,[1] Olivier de Viron,[2] Ichiro Fukumori[1]

Earth's dynamic oblateness (J_2) has been decreasing due to postglacial rebound (PGR). However, J_2 began to increase in 1997, indicating a pronounced global-scale mass redistribution within Earth's system. We have determined that the observed increases in J_2 are caused primarily by a recent surge in subpolar glacial melting and by mass shifts in the Southern, Pacific, and Indian oceans. When these effects are removed, the residual trend in J_2 (-2.9×10^{-11} year^{-1}) becomes consistent with previous estimates of PGR from satellite and eclipse data. The climatic significance of these rapid shifts in glacial and oceanic mass, however, remains to be investigated.

Earth is a dynamic system; it has a fluid, mobile atmosphere and oceans; a continually changing global distribution of ice, snow, and ground water; a fluid core that is undergoing hydromagnetic motion; a mantle that is thermally convecting and rebounding from the glacial loading of the last Ice Age; and mobile tectonic plates. These processes modify the distribution of Earth system mass and, consequently, affect its gravitational field over time and space. By investigating interannual and decadal changes in Earth's gravity field, insights into processes involving large-scale mass transport (*1*) on these time scales can be gained. Here, we investigate changes in the Earth's dynamic oblateness, J_2 [defined in (*2*)], a dimensionless coefficient of the degree 2, order 0 spherical harmonic component of the gravity field, which has its maximum at the equator and symmetric minima at the poles.

Earth's oblateness has been decreasing steadily, as originally revealed by satellite laser ranging (SLR) data beginning in 1979 (*3*) and subsequently confirmed by analysis of eclipse records dating back some 2500 years (*4*). This secular trend in J_2 arises primarily from postglacial rebound (PGR), the continuing slow response of the mantle to the last major deglaciation (18,000 to 6000 years before the present). Recently, however, Cox and Chao (*5*) used a multisatellite solution to show that J_2 has been increasing since 1997 (Fig. 1A), implying an equatorward mass redistribution in Earth's system strong enough to reverse the negative trend due to PGR. They suggested a variety of sources for the implied mass shift, including the polar ice sheets (Greenland and Antarctica), subpolar and mountain glaciers, the oceans, and Earth's fluid outer core, but left open the question of a climatic origin for the observed trend reversal in J_2 (*5*, *6*).

Here, we systematically explore possible sources of mass redistribution, specifically considering the oceans, land ice systems, the atmosphere, and groundwater. Because the J_2 change coincides with the strong 1997–98 El Niño–Southern Oscillaion (ENSO) event and a marked shift in the index of the Pacific Decadal Oscillation (PDO) (*5*–*7*), the ocean is a prime candidate for examination. The assimilation of satellite sea-surface height measurements with other data types into advanced ocean general circulation models (OGCMs) holds promise for unraveling the oceans' effect on Earth's gravity. We use a state-of-the-art OGCM with assimilated TOPEX/Poseidon (T/P) sea level and expendable bathythermograph (XBT) temperature profile data to assess the oceanic contribution to the observed changes in J_2 [(Fig. 1B), calculated (*2*) from bottom pressure analyses of the Consortium for "Estimating the Circulation and Climate of the Ocean" (ECCO) (*8*)].

Due to its concentration at high latitude, mass changes in land ice can strongly impact Earth oblateness (changes in nongrounded sea ice do not directly affect J_2). The polar ice sheets contain the largest reservoir of land ice, but their mass balances are subject to climate forcing over a broad range of time scales and are not presently well known (*9*). The smaller subpolar and mountain glaciers constitute a tiny fraction (<1%) of Earth's grounded ice, but they may be more sensitive to interannual and decadal climate forcing and have been extensively studied (*10*–*12*). We examine the impact of changes in their global mass balance compiled by the National Snow and Ice Data Center (NSIDC) (*13*) for the years 1961–1998 [(Fig. 1C), calculated with a J_2 scaling of 0.63×10^{-11} per 100 km^3 equivalent volume of meltwater (*14*, *15*)]; extrapolation of the glacial source term beyond 1998 is discussed below.

Atmospheric effects on J_2 (Fig. 1D) were calculated (*2*) from National Centers for Environmental Prediction (NCEP) reanalysis data (*16*) with the use of the inverted barometer (IB) assumption (*17*), with surface pressure data from Antarctica excluded (*18*–*20*). Groundwater effects on J_2 (Fig. 1E) were also calculated (*2*) from NCEP reanalysis data. Note that the atmospheric and groundwater contributions were essentially flat or decreasing after 1997, whereas the geodetic, oceanic, and glacial series all showed pronounced increases in slope at about this time.

If all influences other than PGR were removed, J_2 should have a uniform linear trend over the analysis period considered here, which is much shorter than the characteristic time scales for mantle rebound (*14*). To quantify the origins of nonlinear behavior in the J_2 data, we calculated the variance explained by linear and quadratic fits to the observations and to the residual series obtained by subtraction of the sources (Fig. 1, B to E). The geodetic J_2 series shows strong nonlinearity (Fig. 2A), with a

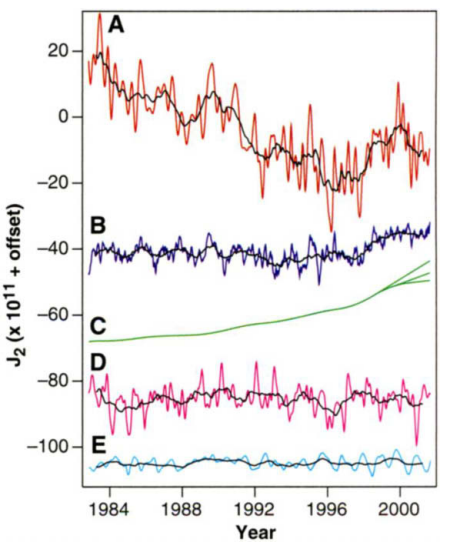

Fig. 1. J_2 observations and source terms, considered for October 1982 to September 2001. **(A)** Geodetic observations (*5*). Earlier data were omitted due to their larger formal uncertainties. **(B)** Integrated oceanic effects from ECCO OGCM analyses (*8*) with T/P and XBT data assimilated beginning in 1993. **(C)** Subpolar glacial effects (*13*–*15*) with three post-1998 melting scenarios (see SOM Text and table S1). **(D)** Integrated atmospheric effects from NCEP reanalysis data (*16*) with the IB assumption applied (*17*) and data from Antarctica excluded (*18*). **(E)** Integrated groundwater effects from NCEP reanalysis data. Color lines show monthly interpolation or moving averages, and black lines show annual averages; all series have had composite seasonal cycles and arbitrary vertical offsets removed. Units are 10^{-11}.

[1]Jet Propulsion Laboratory, California Institute of Technology, Pasadena, CA 91109, USA. [2]Royal Observatory of Belgium/FNRS, B-1180 Brussels, Belgium.

*To whom correspondence should be addressed. E-mail: jean.o.dickey@jpl.nasa.gov

linear fit explaining only 50.2% of the variance and the quadratic term (a measure of residual nonlinearity) accounting for an additional 10.6% (Table 1). Removal of oceanic effects computed from a run of the ECCO model with no data assimilation produces a substantial increase in the linear variance of the J_2 residual, along with a decrease in the variance explained by adding the quadratic term (Table 1). Assimilation of T/P and XBT data into the ocean model beginning in 1993 further reduces the nonlinearity of the J_2 residual (Fig. 2B). A linear fit accounts for 65.4% of the variance and the quadratic term only an additional 3.7%, after subtracting the assimilated ocean model effects. The assimilation's improvements provide a demonstration of the significance of the oceanographic observations and the fidelity of the data assimilation system.

The model change in average ocean bottom pressure between the years 1996–97 and 1999–2000 (Fig. 3) shows the geographical pattern of mass redistribution (*21*) that caused the marked rise in oceanic J_2 which occurred around 1998 (Fig. 1B). Positive anomalies in the Indian Ocean and negative anomalies in the Southern Ocean indicate a pronounced equatorward shift of oceanic mass; because these anomalies are predominantly located on opposite sides of the J_2 nodal line at 35.3°S, they both contributed in a positive sense to the change in dynamic oblateness during 1998 (*2*). A substantial J_2 contribution also comes from the tropical Pacific, where smaller bottom pressure enhancements are spread over a wider area. A more detailed look at changes in oceanic mass and J_2 forcing as a function of latitude is provided in fig. S1 and S2.

Most of the remaining nonlinearity in the J_2 residual is accounted for by removal of the subpolar glacial effects (Fig. 1C). During the decade 1980–89, the glacial J_2 contribution was nearly linear with a slope of about 0.6×10^{-11} year^{-1}, reflecting an average melting rate of about 100 km^3 year^{-1} (*5*, *13*, *14*). In the 1990's, the melting rate accelerated, with sharp increases to 320 km^3 in 1997 and 540 km^3 in 1998 (the last year of the NSIDC global mass balance record). The upper branch of Fig. 1C (ICEHI) assumes constant melting at this rate for the remainder of the analysis, the middle branch (ICE) assumes a return to the smaller 1997 rate in the following year (1999), and the lower branch (ICELO) assumes a further decrease to the 1996 melting rate (120 km^3) in the year 2000 (table S1). Each of these scenarios accounts for virtually all of the remaining quadratic variance in the residual J_2 series (Table 1). Because the ICEHI scenario yields the largest linear variance (85.5%) in the corresponding J_2 residual (Fig. 2C), it is used in the remainder of the analysis.

In keeping with their relative lack of long-term variability (Fig. 1, D and E), removal of the atmospheric and groundwater effects produces little change in the trend of the J_2 residual (Fig. 2, D and E), and only minor increases in explained variance (Table 1). The residual J_2 slope after removal of all sources considered is $dJ_2/dt = -2.9 \times 10^{-11}$ year^{-1}, which is compatible with previous SLR estimates (SOM references *S3*–*S13*). The secular trend in Earth's long-wavelength gravity field is a sensitive indicator of its rheology (*22*), which governs such fundamental processes as mantle convection and plate tectonics. Our results are consistent with relatively moderate values of deep mantle viscosity (~2 x 10^{21} Pa s) (*23*), although a substantial J_2 contribution from ablating polar ice sheets would admit a larger range of viscosity estimates (*14*, *24*). Lastly, we note that the difference in slopes between the pre-1998 and full J_2 residuals in Fig. 2E ($0.15 \times$

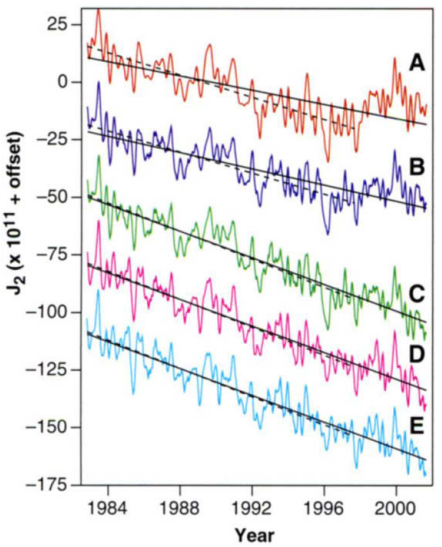

Fig. 2. J_2 observations and residuals (**A** to **E**), obtained by successive removal of the source terms shown in Fig. 1, with 2-month moving averages and arbitrary vertical offsets applied. Solid black lines show linear fits to the series for October 1982 to September 2001; dashed lines show fits for the series to 1997. The ICEHI scenario (see SOM Text and table S1) was used to compute the glacial effect on J_2. Units are 10^{-11}.

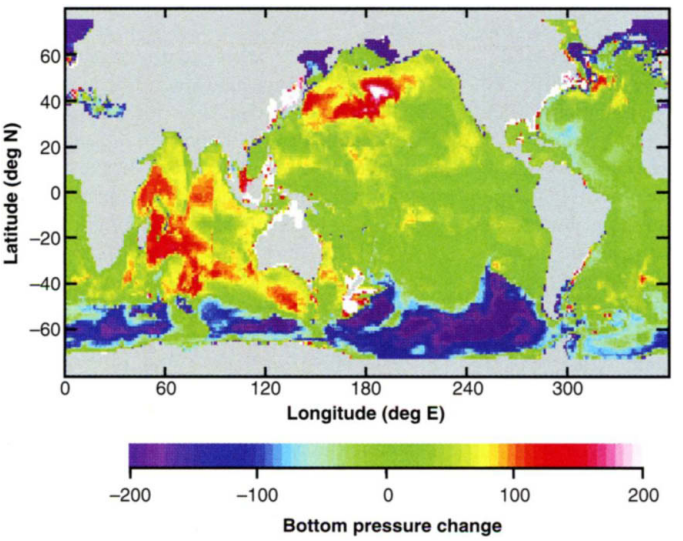

Fig. 3. Change of average bottom pressure (*21*) in the assimilated ocean model (*8*, *15*), between the years 1996–97 and 1999–2000. A pronounced meridional shift in mass from the Southern Ocean to the Pacific and Indian Oceans accounts for most of the increase in oceanic J_2 during 1998 (see also Fig. 1B and figs. S1 and S2). Units are Nm^{-2}.

Table 1. Linear slope and variance explained by linear and quadratic fits to the J_2 observations and residuals, and the additional variance explained by the quadratic fit. O (na) and O (as) denote the nonassimilated and assimilated ocean results, respectively; I (lo), I, and I (hi) denote the ICELO, ICE, and ICEHI melting scenarios, respectively (table S1); and A and G denote atmospheric and groundwater effects, respectively. Smoothing is as in Fig. 2.

	Degree 1		Degree 2	
	Slope 10^{-11} year^{-1}	Variance explained (%)	Variance explained (%)	Variance difference (%)
J_2 (observed)	−1.54	50.2	60.8	10.6
J_2 − O (na)	−1.77	61.3	68.9	7.6
J_2 − O (as)	−1.75	65.4	69.1	3.7
J_2 − O (as) − I (lo)	−2.77	84.4	84.6	0.2
J_2 − O (as) − I	−2.81	84.7	84.8	0.1
J_2 − O (as) − I (hi)	−2.88	85.5	85.6	0.1
J_2 − O (as) − I (hi) − A	−2.87	86.3	86.4	0.1
J_2 − O (as) − I (hi) − A − G	−2.90	86.6	86.8	0.2

10^{-11} year^{-1}) is less than the uncertainty in the J_2 rate given by (*5*), confirming that the climatic effects considered here account for the observed change in J_2 slope within the uncertainty of the observations.

In summary, our findings demonstrate that the J_2 slope reversal observed in 1997–98 (*5*) was the result of dramatic changes in oceanic and glacial mass distribution at that time. Our modeling results show that an equatorward mass shift in the oceans contributed a substantial portion of the J_2 increase during 1998 (Figs. 1B and 2B; figs. S1 and S2), coincident with phase reversals in both ENSO and the PDO. The year 1998 also saw the warmest global mean surface temperature on record (*25*), and we found that a concomitant surge in subpolar glacial melting (*13*, *26*) can account for nearly all of the remaining nonlinear behavior in the J_2 observations (Figs. 1C and 2C; Table 1). However, the dynamical links between these relatively rapid mass shifts and concurrent climate anomalies remain to be established. Further knowledge of Earth system processes, in particular polar ice sheet ablation (*27*), is needed to form a more comprehensive picture of ongoing mass balance changes and their climatic origins. New sources of geodetic data, such as the monthly time-variable gravity fields to be supplied by the recently launched GRACE mission (*28*), may soon revolutionize our ability to monitor and interpret these changes.

References and Notes

1. J. O. Dickey *et al.*, *Satellite Gravity and the Geosphere* (National Research Council, Washington, DC, 1997).
2. The definition and method of calculation for J_2 are given in the SOM Text.
3. C. F. Yoder *et al.*, *Nature* **307**, 757 (1983).
4. F. R. Stephenson, L. V. Morrison, *Philos. Trans. R. Soc. A* **351**, 165 (1995).
5. C. M. Cox, B. F. Chao, *Science* **297**, 831 (2002).
6. A. Cazenave, R. S. Nerem, *Science* **297**, 783 (2002).
7. S. R. Hare, N. J. Mantua, *Progr. Oceanogr.* **47**, 103 (2000).
8. T/P and XBT data were assimilated into the model run starting in 1993. Further details regarding the ECCO assimilation system are available at www.ecco-group.org. A brief summary is given in the SOM Text.
9. E. Rignot, R. H. Thomas, *Science* **297**, 1502 (2002).
10. M. B. Dyurgerov, M. F. Meier, *Arct. Alpine Res.* **29**, 379 (1997).
11. ———, *Arct. Alpine Res.* **29**, 392 (1997).
12. ———, *Proc. Natl. Acad. Sci. U.S.A.* **97**, 1406 (2000).
13. Annual volume changes in subpolar and mountain glaciers were obtained from the NSIDC Web site www-nsidc.colorado.edu/sotc/glacier_balance.html, courtesy of M. Dyurgerov, Institute of Arctic and Alpine Research, University of Colorado, Boulder.
14. T. S. James, E. R. Ivins, *J. Geophys. Res.* **102**, 605 (1997).
15. Glacial contributions to sea level change are not included in the ocean model, which is constrained to have constant volume (Boussinesq approximation). Before computing the oceanic J_2 contribution, the model bottom pressures are adjusted uniformly such that the global ocean mass is time-invariant.
16. E. M. Kalnay *et al.*, *Bull. Am. Meteorol. Soc.* **77**, 437 (1996).
17. The IB assumption accounts for oceanic compensation of atmospheric loading by substituting a spatially averaged uniform surface pressure field over the global ocean.
18. Because atmospheric pressure trends over Antarctica are poorly constrained due to a lack of data and calibration problems (*19*, *20*), we extended the IB assumption to include the land surface of Antarctica in this study.
19. K. M. Hines, D. H. Bromwich, G. J. Marshall, *J. Clim.* **13**, 3940 (2000).
20. G. J. Marshall, *J. Clim.* **15**, 659 (2002).
21. The model bottom pressure is directly proportional to the mass-per-unit area above a given point.
22. P. Johnston, K. Lambeck, *Geophys. J. Int.* **136**, 537 (1999).
23. R. Devoti *et al.*, *Geophys. Res. Lett.* **28**, 855 (2001).
24. R. Sabadini, B. L. A. Vermeersen, in *Ice Sheets, Sea Level and the Dynamic Earth*, vol. 29 of Geodynamics Series, J. X. Mitrovica, B. L. A. Vermeersen, Eds. (American Geophysical Union, Washington, DC, 2002).
25. J. Hansen *et al.*, *J. Geophys. Res.* **104**, 30,997 (1999).
26. J. Oerlemans, *Ann. Glaciol.* **31**, 44 (2000).
27. H. J. Zwally *et al.*, *Science* **297**, 218 (2002).
28. D. Adam, *Nature* **416**, 10 (2002)

29. The authors gratefully acknowledge discussions (both oral and via e-mail) with J.-P. Boy, D. Bromwich, B. F. Chao, Y. Chao, C. M. Cox, M. B. Dyurgerov, L.-L. Fu, M. Ghil, E. Ivins, K. Mo, and Y.Yung, and the constructive comments of the reviewers. The work of J.O.D., S.L.M., and I.F. presents the results of one phase of research carried out at the Jet Propulsion Laboratory, under contract with the National Aeronautics and Space Administration. O.D.V. is a postdoctoral researcher of the National Fund for Scientific Research, Belgium. This work was accomplished during O.D.V.'s visit to JPL during Summer 2002. This is a contribution of the ECCO consortium funded by the National Oceanographic Partnership Program.

Supporting Online Material

www.sciencemag.org/cgi/content/full/298/5600/1975/DC1

Materials and Methods
SOM Text
Figs. S1 and S2
Table S1
References and Notes

27 August 2002; 4 November 2002

Environmental Effects of Large Impacts on Mars

Teresa L. Segura,[1]*† Owen B. Toon,[1] Anthony Colaprete,[2] Kevin Zahnle[2]

The martian valley networks formed near the end of the period of heavy bombardment of the inner solar system, about 3.5 billion years ago. The largest impacts produced global blankets of very hot ejecta, ranging in thickness from meters to hundreds of meters. Our simulations indicated that the ejecta warmed the surface, keeping it above the freezing point of water for periods ranging from decades to millennia, depending on impactor size, and caused shallow subsurface or polar ice to evaporate or melt. Large impacts also injected steam into the atmosphere from the craters or from water innate to the impactors. From all sources, a typical 100-, 200-, or 250-kilometers asteroid injected about 2, 9, or 16 meters, respectively, of precipitable water into the atmosphere, which eventually rained out at a rate of about 2 meters per year. The rains from a large impact formed rivers and contributed to recharging aquifers.

The valley networks on Mars cut across the heavily cratered southern highlands, the oldest terrain on the planet, signifying that they are contemporaneous with the period of heavy cometary and asteroidal bombardment of Mars and of the rest of the inner solar system (*1*, *2*). There are about 25 visible craters with diameters between 600 and 4000 km (fig. S1) (*3*). Many other large craters may have been erased by resurfacing events (*4*). Here we consider how impacts might have caused water to flow on Mars and create the valley networks.

An asteroid (*5*) with a diameter of 100 (200, 250) km and traveling at 9 km/s delivers about 6×10^{25} (4×10^{26}, 9×10^{26}) J of energy to the planet and generates a crater ~600 (1000, 1300) km in diameter (fig. S1) and 3×10^{18} (3×10^{19}, 5×10^{19}) kg of ejecta (*6*–*8*) (Fig. 1). Ejecta include vaporized and melted impactor and target materials. About 20% of the ejecta are rock vapors (*6*); most of the rest is melt (*7*). Only a few percent of the ejecta mass would escape from Mars, given a 9 km/s impact velocity (*6*). In the case of large impacts, the ejecta are hot because of the large energy release and because of the low surface-to-volume ratio of the ejecta, which inhibits cooling. The hot ejecta are distributed globally both ballistically and via the thermally expanding vapor cloud. For a time, the rock vapor is suspended in the hot atmosphere because it is too warm to condense immediately.

There are several primary sources of water. The impactor itself may deliver water. A 100 (200, 250)-km asteroid that is 5% water by mass (*8*) would deliver 40 (310, 620) cm

[1]Program in Atmospheric and Oceanic Sciences, Laboratory for Atmospheric and Space Physics, University of Colorado, Campus Box 392, Boulder, CO 80309–0392, USA. [2]NASA-Ames Research Center, MS 245-3, Moffett Field, CA 94035, USA.

*Present address: NASA-Ames Research Center, MS 245-3, Moffett Field, CA 94035, USA.
†To whom correspondence should be addressed.